Rail. Eng. Science (2022) 30(4):468–481
https://doi.org/10.1007/s40534-022-00276-z

A substructure approach for analyzing pile foundation and soil vibrations due to train running over viaduct and its validation

Ying Wu[1] · Xuecheng Bian[1] · Chong Cheng[1] · Jianqun Jiang[1]

Received: 28 December 2021 / Revised: 6 May 2022 / Accepted: 7 May 2022 / Published online: 5 July 2022

Abstract An efficient computational approach based on substructure methodology is proposed to analyze the viaduct–pile foundation–soil dynamic interaction under train loads. The train–viaduct subsystem is solved using the dynamic stiffness integration method, and its accuracy is verified by the existing analytical solution for a moving vehicle on a simply supported beam. For the pile foundation–soil subsystem, the geometric and material properties of piles and soils are assumed to be invariable along the azimuth direction. By introducing the equivalent stiffness of grouped piles, the governing equations of pile foundation–soil interaction are simplified based on Fourier decomposition method, so the three-dimensional problem is decomposed into several two-dimensional axisymmetric finite element models. The pile foundation–soil interaction model is verified by field measurements due to shaker loading at pile foundation top. In addition, these two substructures are coupled with the displacement compatibility condition at interface of pier bottom and pile foundation top. Finally, the proposed train–viaduct–pile foundation–soil interaction model was validated by field tests. The results show that the proposed model can predict vibrations of pile foundation and soil accurately, thereby providing a basis for the prediction of pile–soil foundation settlement. The frequency spectra of the vibration in Beijing–Tianjin high-speed railway demonstrated that the main frequencies of the pier top and ground surface are below 100 and 30 Hz, respectively.

✉ Xuecheng Bian
bianxc@zju.edu.cn

[1] Department of Civil Engineering, MOE Key Laboratory of Soft Soils and Geoenvironmental Engineering, Zhejiang University, Anzhong Building of Civil Engineering B406, Zijingang Campus, Hangzhou 310058, China

Keywords Train moving load · Viaduct · Pile foundation · Soil · Vibration · Substructure method

1 Introduction

Pile-supported viaducts are widely used in high-speed railways across soft soil deposited areas or densely populated urban areas. In China, viaducts are used in more than 70% of newly built high-speed railways. When trains pass through urban areas, the ground vibrations induced by trains running over viaducts transmit to the surrounding buildings due to the interaction between the soil and the structure, leading to serious noise interference and surrounding ground settlement, which brings detrimental effects to people's work and lives. There are many studies on the environmental noise problem; for example, in Refs. [1–3], the researchers proposed some theoretical models to predict the environmental noise generated by trains passing through viaducts and discussed noise reduction measures. However, less attention was paid to the prediction and evaluation of settlement caused by ground vibrations due to trains running on viaducts. To this end, it is necessary to build a train–viaduct–pile foundation–soil interaction model to predict effectively the vibrations of pile foundation and soil.

To date, much work has been done to study train–bridge (viaduct) dynamic interaction for the purposes of safe train operation and railway structure design. Frýba [4] derived an analytical solution for the beam structure subjected to a moving load. Yang et al. [5] simplified train as a series of moving load to investigate parameters that control the dynamic bridge responses, such as bridge's span length, car length, and train speed. Zeng et al. [6] proposed a train–track–bridge coupled dynamics modeling method which greatly reduces the matrix dimension and computer

performance requirements. Gou et al. [7] studied the dynamic responses of a long-span cable-stayed railway bridge with steel–concrete hybrid girders in different train load scenarios through in situ testing. Cheng et al. [8–10] proposed a bridge–track–vehicle element for analyzing vibrations of railway bridges under a moving train, which shows that bridge vibration has a significant effect on the dynamic response of railway track.

The foregoing studies on train–bridge (viaduct) dynamics provide theoretical basics for understanding train–viaduct dynamic interaction and vibration generation. So far, train-induced ground vibrations have been widely studied, but most of the published works focus on vibrations induced by trains running on ground surface [11–14], and very limited literature is available on ground vibrations induced by train running on viaduct [15–18]. Zhang et al. [15] proposed a semi-analytical model to investigate structure and ground-borne vibrations caused by trains running over viaducts, taken into consideration the vibration-isolating effects of the multi-layered elastic supports. Shi et al. [16] presented a theoretical evaluation on vibrations of saturated ground induced by high-speed train operating on an elevated bridge and identified two characteristic frequencies of the superstructure that dominates the ground displacement response. In addition, Takemiya and Bian [17] proposed a substructure method to study the ground vibration induced by Shinkansen train and validated it with field measurements. Fujikake [18] proposed a vehicle–bridge–ground dynamic interaction model to investigate the environment vibration along Shinkansen railway and analyzed vibration characteristics of the bridge structure and alongside soil.

In the literature, most analyses on bridge–pile–soil interaction under the excitation of trains fall into two categories: (1) simplified analytical solution and (2) fully three-dimensional numerical model. The simplified analytical solution can get the vibration results of a bridge and its nearby ground at a very low computational cost and get insight into structure vibration and propagation in soil. But this kind of models usually imposed some assumptions on bridge structure, pile foundation, and soil, so they can be described by simple analytical formulations. The fully three-dimensional finite models can well describe the details of bridge, pile foundation, and ground soil and incorporate more realistic material attributes, but computations of these numerical models are very time-consuming, which prevents its application in engineering.

In this paper, the coupled viaduct–pile foundation–soil dynamic interaction system is divided into two subsystems based on the dynamic substructure method. The train–viaduct subsystem is solved by dynamic stiffness integration method, and the pile foundation–soil subsystem is solved using Fourier series decomposition in the azimuth direction. The two subsystems are coupled with the displacement compatibility condition at the interface of viaduct pier bottom and pile foundation top. After the models of the two subsystems are verified, they are integrated to analyze the coupled viaduct–pile foundation–soil interaction under train moving load. Finally, field test validation was used to demonstrate the applicability of the proposed analysis model in predicting high-speed train induced structure and ground vibrations.

2 Methodology

The finite element method (FEM) can deal with the complex geometry of viaduct and pile foundation effectively, but the full three-dimensional finite element model of viaduct–pile foundation–soil with dynamic excitation of train loadings can be very computationally expensive since the ground is infinite in nature. The whole viaduct–pile foundation–soil system with train moving load is shown in Fig. 1. It can be divided into two subsystems based on dynamic substructure method to reduce the computation complexity. One is the train–viaduct subsystem, and the other is the pile foundation–soil subsystem. By assuming that the interface of viaduct pier and pile foundation is in close contact, these two subsystems are coupled with the displacement continuity condition at interface. All of these solutions take place in the frequency domain, since some important parameters controlling structure and soil vibrations are more accurately and easily identified in the frequency domain, such as the impedance functions and damping. The time histories of viaduct and ground vibrations are then obtained by the inverse Fourier transform from the counterpart solution.

Several steps are required for solving the whole dynamic system based on the substructure method. The methodology flow chart is shown in Fig. 2. First, the impedance function of pile foundation is derived from the pile foundation–soil interaction, and the transfer function of vibration transmission from pile foundation to surrounding soil is determined. The impedance function of pile foundation is integrated into viaduct governing equations at all pier

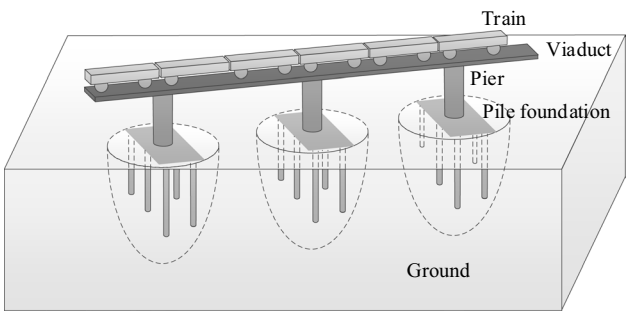

Fig. 1 Train–viaduct–pile foundation–soil interaction model

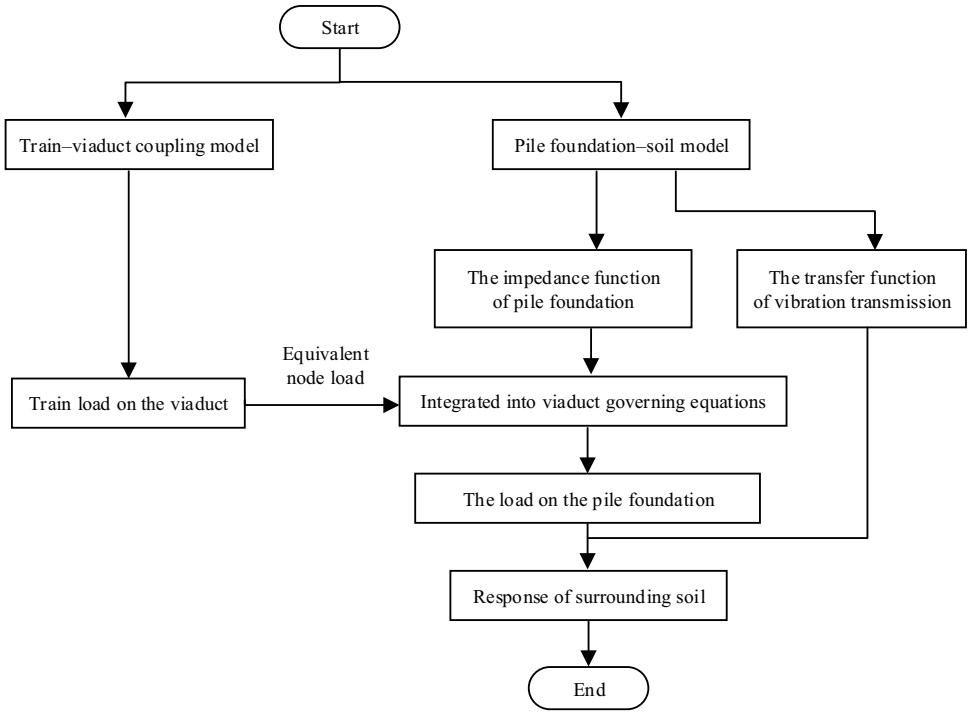

Fig. 2 Flow chart of the methodology

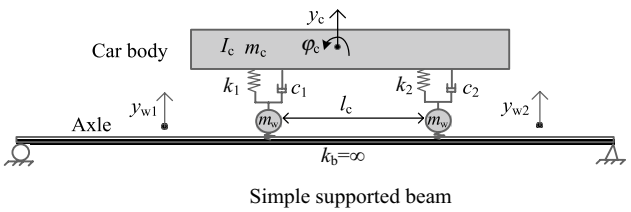

Fig. 3 Train–beam coupling model

bottoms. After solving the governing equation of viaduct under train moving load, the loadings acting on pile foundation top can be retrieved and are used in computation of ground vibration based on the transfer function derived in the first step.

3 Interaction model of moving train on viaduct supported by pile foundation

3.1 Train–viaduct coupling model

In this study, the train car is modeled as a multi-rigid body and its motions are represented by 4 degrees of freedom (DOFs) in the vertical plane, as shown in Fig. 3. Although such simplification can affect the response of ground vibration in high frequency domain, it has negligible influence on the subsequent calculation of pile foundation–soil settlement. The dynamic wheel–rail force and fastener force due to track irregularity mostly affect track dynamic responses in high-frequency band and decays faster, so it has little influence on the pile settlement and the dynamic response of far field. In order to develop a simplified model to predict the pile foundation–soil settlement, the track irregularity is not considered here. The motions of the train car include vertical displacements of the car body and two wheels, and the rotation of the car body. The suspensions of the car body are simplified as primary springs with constants k_1 and k_2 and dashpots with damping coefficients c_1 and c_2, respectively. The masses of car body and wheels are represented by m_c and m_w and their vertical movements by y_c and y_w, respectively. The torsion angle and wheelbase are denoted by φ_c and l_c, respectively. The beam stiffness and moment inertia of the car body are denoted by k_b and I_c, respectively.

The motion of train car can be described by the following governing equation:

$$\boldsymbol{M}_v\ddot{\boldsymbol{y}}_v + \boldsymbol{C}_v\dot{\boldsymbol{y}}_v + \boldsymbol{K}_v\boldsymbol{y}_v = \boldsymbol{f}_v, \tag{1}$$

where $\boldsymbol{K}_v$, $\boldsymbol{C}_v$, and $\boldsymbol{M}_v$ are stiffness matrix, damping matrix and mass matrix of car body; $\boldsymbol{y}_v$ is displacement vector; and $\boldsymbol{f}_v$ is force vector. Their detailed expressions are given as below:

$$\boldsymbol{K}_{\mathrm{v}}=\begin{bmatrix} \frac{k_1 l_{\mathrm{c}}^2}{2} & & & \\ 0 & 2k_1 & & \\ -\frac{k_1 l_{\mathrm{c}}}{2} & -k_1 & k_1 & \\ \frac{k_1 l_{\mathrm{c}}}{2} & -k_1 & 0 & k_1 \end{bmatrix},\ \boldsymbol{C}_{\mathrm{v}}=\begin{bmatrix} \frac{c_1 l_{\mathrm{c}}^2}{2} & & & \\ 0 & 2c_1 & & \\ -\frac{c_1 l_{\mathrm{c}}}{2} & -c_1 & c_1 & \\ \frac{k_1 l_{\mathrm{c}}}{2} & -c_1 & 0 & c_1 \end{bmatrix},$$

$$\boldsymbol{M}_{\mathrm{v}}=\begin{bmatrix} I_{\mathrm{c}} & & & \\ 0 & m_{\mathrm{c}} & & \\ 0 & 0 & m_{\mathrm{w}} & \\ 0 & 0 & 0 & m_{\mathrm{w}} \end{bmatrix},\ \boldsymbol{y}_{\mathrm{v}}=\begin{pmatrix} \varphi_{\mathrm{c}} \\ y_{\mathrm{c}} \\ y_{\mathrm{w1}} \\ y_{\mathrm{w2}} \end{pmatrix},$$

in which $\boldsymbol{K}_{\mathrm{v}}$, $\boldsymbol{C}_{\mathrm{v}}$, and $\boldsymbol{M}_{\mathrm{v}}$ are symmetric matrices.

In this study, the train load on the viaduct is obtained by solving Eq. (1); then, it is substituted into the viaduct's governing equation (i.e., Eq. (2)) as the equivalent node load in the frequency domain, for which one can refer to the author's previous work [17]. The vertical displacement at wheel–viaduct contact position is approximated by linear interpolation of the neighboring two nodes on viaduct.

The model of a moving vehicle on a simply supported beam is used to verify the proposed train–viaduct dynamic interaction analysis model, as shown in Fig. 3, since there is an analytical solution available in Ref. [4]. Parameters of the train car and beam are given in Table 1. As shown in Figs. 4 and 5, the developed model shows good agreement with Frýba's analytical solution [4], both for the vibrations of beam center and car body center.

3.2 Modeling of viaduct structure supported by pile foundation

The viaduct deck and piers are modeled by three-dimensional beam elements. The track, including rails, fastener, and underlying slab layer, is condensed into the stiffness of viaduct deck. The supporting of pile foundation to viaduct is represented by frequency-dependent impedance functions.

The governing equation of the viaduct with multiple pier supports is formulated in frequency as follows:

$$-\omega^2\boldsymbol{M}\boldsymbol{U}^{\mathrm{t}}+\mathrm{i}\omega\boldsymbol{C}\boldsymbol{U}^{\mathrm{t}}+\boldsymbol{K}\boldsymbol{U}^{\mathrm{t}}=\boldsymbol{F}^{\mathrm{t}}, \tag{2}$$

where $\boldsymbol{M}$, $\boldsymbol{C}$, and $\boldsymbol{K}$ are the mass, damping, and stiffness matrices, respectively; $\boldsymbol{U}^{\mathrm{t}}$ is the displacement matrix; $\boldsymbol{F}^{\mathrm{t}}$ is the force vector; ω denotes angular frequency and i the imaginary unit.

By separating the displacement and load vectors at superstructure nodes (denoted by subscript 's') and at interface nodes at pier bottoms (denoted by subscript 'i'), Eq. (2) is rewritten as

Table 1 Parameters of train car and beam

Parameter	Value
Train speed v	20 m/s
Beam span L	40 m
Beam weight G	1.14×10^5 kg
Young's modulus of the beam E_{b}	2×10^{11} Pa
Wheelbase l_{c}	17.5 m
Mass of car body m_{c}	2×10^4 kg
Mass of wheel m_{w}	1×10^3 kg
Moment inertia of car body I_{c}	1×10^5 kg·m^2
Stiffness of primary suspension k_1, k_2	1 MN/m
Damping of primary suspension c_1, c_2	50 kN·s/m

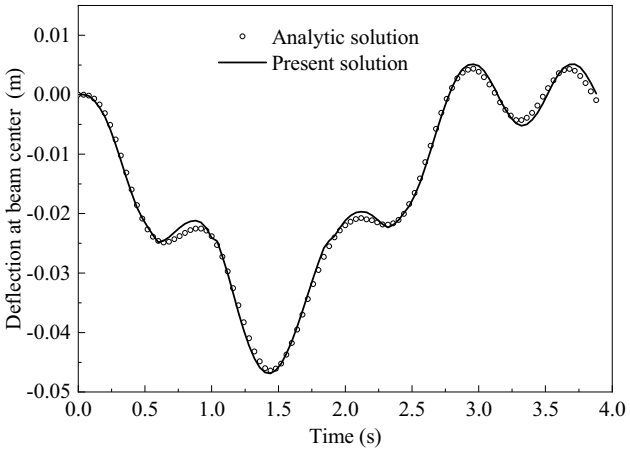

Fig. 4 Vibration at beam center

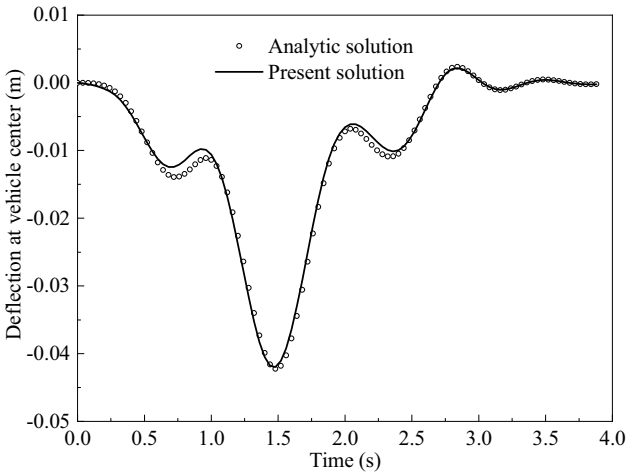

Fig. 5 Vibration at car body center

$$-\omega^2\begin{bmatrix}\boldsymbol{M}_{ss} & \boldsymbol{M}_{si}\\ \boldsymbol{M}_{is} & \boldsymbol{M}_{ii}\end{bmatrix}\begin{Bmatrix}\boldsymbol{U}_s^t\\ \boldsymbol{U}_i^t\end{Bmatrix}+\mathrm{i}\omega\begin{bmatrix}\boldsymbol{C}_{ss} & \boldsymbol{C}_{si}\\ \boldsymbol{C}_{is} & \boldsymbol{C}_{ii}\end{bmatrix}\begin{Bmatrix}\boldsymbol{U}_s^t\\ \boldsymbol{U}_i^t\end{Bmatrix}+\begin{bmatrix}\boldsymbol{K}_{ss} & \boldsymbol{K}_{si}\\ \boldsymbol{K}_{is} & \boldsymbol{K}_{ii}\end{bmatrix}\begin{Bmatrix}\boldsymbol{U}_s^t\\ \boldsymbol{U}_i^t\end{Bmatrix}=\begin{Bmatrix}\boldsymbol{F}_s^t\\ \boldsymbol{F}_i^t\end{Bmatrix}, \tag{3}$$

where the matrixes with subscripts ''ss'' and ''ii'' denote the self-matrices of the train–viaduct subsystem and pile foundation–soil subsystem, respectively, and the ones with subscripts ''si'' and ''is'' denote the interaction matrices between subsystems.

Here, $\boldsymbol{F}^t$ is only the train load on the viaduct, and it is not a stationary process. The train load $\boldsymbol{F}^t$ can be obtained by solving Eq. (1), and then, it is substituted into the viaduct's governing equation (i.e., Eq. (2)) as equivalent node load in the frequency domain. Thus, the global dynamic equations of viaduct structure are expressed as

$$-\omega^2\begin{bmatrix}\boldsymbol{M}_{ss} & \boldsymbol{M}_{si}\\ \boldsymbol{M}_{is} & \boldsymbol{M}_{ii}\end{bmatrix}\begin{Bmatrix}\boldsymbol{U}_s^t\\ \boldsymbol{U}_i^t\end{Bmatrix}+\mathrm{i}\omega\begin{bmatrix}\boldsymbol{C}_{ss} & \boldsymbol{C}_{si}\\ \boldsymbol{C}_{is} & \boldsymbol{C}_{ii}\end{bmatrix}\begin{Bmatrix}\boldsymbol{U}_s^t\\ \boldsymbol{U}_i^t\end{Bmatrix}+\begin{bmatrix}\boldsymbol{K}_{ss} & \boldsymbol{K}_{si}\\ \boldsymbol{K}_{is} & \boldsymbol{K}_{ii}+\boldsymbol{K}_f\end{bmatrix}\begin{Bmatrix}\boldsymbol{U}_s^t\\ \boldsymbol{U}_i^t\end{Bmatrix}=\begin{Bmatrix}\boldsymbol{F}_s^t\\ 0\end{Bmatrix}, \tag{4}$$

where $\boldsymbol{K}_f$ is the impedance function of pile foundation.

The governing equation of train car movements is integrated into Eq. (4) according to the train–beam interaction model proposed in Sect. 3.1.

4 Modeling of pile–foundation and soil dynamic interaction

4.1 Three-dimensional axisymmetric pile foundation model

Pile foundation is used to support viaduct widely, but the pile foundation–soil interaction has been paid less attention to in previous works. However, soil–structure interaction significantly affects the dynamic response of viaduct under high-speed train loadings [17]. Besides, study on ground vibrations caused by train running over viaduct is another important issue from environmental amenity considerations. Therefore, it is indispensable for soil–pile interaction analysis to determine the vibration propagation from pile foundation to adjacent ground soil. In this regard, semi-analytical solution with axisymmetric FEM is effective to study the dynamic problem of pile foundation with the ring-like arrangement of pile group [19, 20]. Here, we extend this method to study pile–foundation dynamic interaction under loading transferred from viaduct due to train moving loads, as shown in Fig. 6, where F_x, F_z, and M_y denote the horizontal force, vertical force, and bending moment, respectively. One of the basic assumptions is that the geometric and material properties are invariable in the azimuth direction. Then, for the axisymmetric bodies subject to non-axisymmetric loadings, the Fourier expansion is applied for both the displacement and load components. This solution

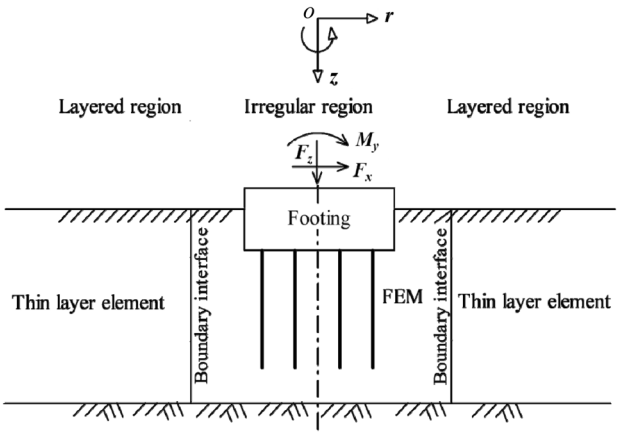

Fig. 6 Pile foundation–soil interaction model

has advantages in saving the memory and computational efforts, compared with the full three-dimensional models.

In this paper, the pile foundations and soil are modeled by three-dimensional axisymmetric finite elements with Fourier expansion about the azimuth. A transmitting boundary based on the thin layer element method [20] is introduced into the analysis to model the infinitely extending layered soil.

For the dynamic problem of pile foundation–soil interaction under train loading on viaduct, displacements and stresses of the pile foundation and surrounding soil do not vary dramatically around the circumference. In this case, the Fourier expansion of the displacement along the circumference is performed and motions of the pile foundation and surrounding soil are approximated expressed by the first several series items.

The ground motions are governed by the Navier–Stokes equations as follows:

$$(\lambda^c+2\mu^c)\nabla(\nabla\cdot\boldsymbol{U})-\mu^c\nabla\times\nabla\times\boldsymbol{U}+\boldsymbol{P}-\rho\ddot{\boldsymbol{U}}=0, \tag{5}$$

where $\boldsymbol{U}$ and $\boldsymbol{P}$ are the soil displacement vector and force vector, respectively; ρ is the soil density; λ^c and μ^c are the Lame constants of the soil including a small part of complex number to consider the ground damping effect and can be expressed as

$$\lambda^c=\lambda(1+2\mathrm{i}\beta),\ \ \mu^c=\mu(1+2\mathrm{i}\beta), \tag{6}$$

where β is the internal damping of soil and the superscript "c" denotes complex number.

The displacement vector $\boldsymbol{U}$ and force vector $\boldsymbol{P}$ can be expressed in cylindrical coordinate system (u, r, θ) using Fourier expansion, as follows:

$$\boldsymbol{U}(r,\theta,z)=\sum_{n=0}^{\infty}\boldsymbol{H}_n^s(\theta)\tilde{\boldsymbol{U}}_n^s(r,z)+\sum_{n=0}^{\infty}\boldsymbol{H}_n^a(\theta)\tilde{\boldsymbol{U}}_n^a(r,z), \tag{7a}$$

$$\boldsymbol{P}(r,\theta,z)=\sum_{n=0}^{\infty}\boldsymbol{H}_n^{\mathrm{s}}(\theta)\tilde{\boldsymbol{P}}_n^{\mathrm{s}}(r,z)+\sum_{n=0}^{\infty}\boldsymbol{H}_n^{\mathrm{a}}(\theta)\tilde{\boldsymbol{P}}_n^{\mathrm{a}}(r,z), \tag{7b}$$

where the Fourier amplitudes $\boldsymbol{U}_n(r,z)$ and the expansion matrix $\boldsymbol{H}_n(\theta)$ are defined as follows:

$$\boldsymbol{U}(r,\theta,z)=(U_r,U_z,U_\theta)^{\mathrm{T}},$$
$$\boldsymbol{U}_n(r,z)=(U_r,U_z,U_\theta)_n^{\mathrm{T}},$$
$$\boldsymbol{H}_n^{\mathrm{s}}(\theta)=\mathrm{diag}(\cos n\theta,-\sin n\theta,\cos n\theta),$$
$$\boldsymbol{H}_n^{\mathrm{a}}(\theta)=\mathrm{diag}(\sin n\theta,\cos n\theta,\sin n\theta);$$

The superscripts 's' and 'a' stand for the symmetric and anti-symmetric terms, respectively. In case of the smoothly deformed configuration, the $n=0$ and 1 terms would be enough to describe the pile and soil responses. Namely, the $n=0$ symmetric harmonic represents a vertical motion in the Z direction as well as a symmetric dilation, while the $n=0$ anti-symmetric harmonic does a torsional motion about the Z axis. The $n=1$ symmetric harmonic relates to a coupled motion of translation along the X axis ($\theta=0^o$) and rotation about the Y axis ($\theta=90^o$), and the $n=1$ anti-symmetric harmonic does a coupled motion of translation along the Y axis and rotation about the X axis. Since the symmetric mode is independent to the anti-symmetric mode, these two motions can be decoupled in the governing equations.

To solve the governing equations for soil vibrations in the finite element model, $\tilde{\boldsymbol{U}}_n^{\mathrm{s}}$ and $\tilde{\boldsymbol{U}}_n^{\mathrm{a}}$ are discretized into finite elements with specific Fourier expansion series. By introducing the shape function $\boldsymbol{N}(r,z)$, the finite element formulation can be deduced by the conventional procedure as

$$\boldsymbol{K}_n\boldsymbol{U}+\boldsymbol{M}_n\ddot{\boldsymbol{U}}=\boldsymbol{P}_n, \tag{8}$$

where $\boldsymbol{K}_n$, $\boldsymbol{M}_n$, and $\boldsymbol{P}_n$ are the stiffness matrix, mass matrix and force vector, respectively, and their detailed formulations are as follows:

$$\boldsymbol{K}_n=\sum_{\text{element}}\left(\alpha_{1n}\iint\boldsymbol{N}^{\mathrm{T}}\boldsymbol{B}_{1n}^{\mathrm{T}}\boldsymbol{D}_1\boldsymbol{B}_{1n}\boldsymbol{N}r\mathrm{d}r\mathrm{d}z+\alpha_{2n}\iint\boldsymbol{N}^{\mathrm{T}}\boldsymbol{B}_{2n}^{\mathrm{T}}\boldsymbol{D}_2\boldsymbol{B}_{2n}\boldsymbol{N}r\mathrm{d}r\mathrm{d}z\right),$$
$$\boldsymbol{M}_n=\sum_{\text{element}}\iint\rho\boldsymbol{N}^{\mathrm{T}}\boldsymbol{\alpha}_n\boldsymbol{N}r\mathrm{d}r\mathrm{d}z,$$
$$\boldsymbol{P}_n=\sum_{\text{elemen}}\left(\iint\boldsymbol{N}^{\mathrm{T}}\boldsymbol{\alpha}_n\boldsymbol{b}_n r\mathrm{d}r\mathrm{d}z+\int_S\boldsymbol{N}^{\mathrm{T}}\boldsymbol{\alpha}_n\boldsymbol{t}_n\mathrm{d}s\right),$$

where the coefficients related to symmetric or anti-symmetric motions are given by

$$\boldsymbol{\alpha}_n^{\mathrm{s}}=\mathrm{diag}\left(\alpha_{1n}^{\mathrm{s}},\alpha_{1n}^{\mathrm{s}},\alpha_{2n}^{\mathrm{s}}\right),\ \boldsymbol{\alpha}_n^{\mathrm{a}}=\mathrm{diag}\left(\alpha_{1n}^{\mathrm{a}},\alpha_{1n}^{\mathrm{a}},\alpha_{2n}^{\mathrm{a}}\right),$$

in which

$$\text{for } n=0\text{: } \alpha_{1n}^{\mathrm{s}}=\alpha_{2n}^{\mathrm{a}}=2\pi,\ \alpha_{2n}^{\mathrm{s}}=\alpha_{1n}^{\mathrm{a}}=0,$$
$$\text{for } n\neq 0\text{: } \alpha_{1n}^{\mathrm{s}}=\alpha_{2n}^{\mathrm{s}}=\alpha_{1n}^{\mathrm{a}}=\alpha_{2n}^{\mathrm{a}}=\pi;$$

$\boldsymbol{b}_n$ is body force; $\boldsymbol{t}_n$ is surface traction; s is arc length; $\boldsymbol{B}_{1n}$, $\boldsymbol{B}_{2n}$, $\boldsymbol{D}_{1,}$ and $\boldsymbol{D}_2$ are matrices defined as

$$\boldsymbol{B}_{1n}=\begin{bmatrix}\frac{\partial}{\partial r}&0&0\\ \frac{1}{r}&0&-\frac{n}{r}\\ 0&0&\frac{\partial}{\partial z}\\ \frac{\partial}{\partial z}&0&\frac{\partial}{\partial r}\end{bmatrix},\ \boldsymbol{B}_{2n}=\begin{bmatrix}\frac{n}{r}&0&-\frac{1}{r}+\frac{\partial}{\partial r}\\ 0&\frac{n}{r}&\frac{\partial}{\partial z}\end{bmatrix},$$

$$\boldsymbol{D}_1=\begin{bmatrix}\lambda^{\mathrm{c}}+2\mu^{\mathrm{c}}&\lambda^{\mathrm{c}}&\lambda^{\mathrm{c}}&0\\ \lambda^{\mathrm{c}}&\lambda^{\mathrm{c}}+2\mu^{\mathrm{c}}&\lambda^{\mathrm{c}}&0\\ \lambda^{\mathrm{c}}&\lambda^{\mathrm{c}}&\lambda^{\mathrm{c}}+2\mu^{\mathrm{c}}&0\\ 0&0&0&\mu^{\mathrm{c}}\end{bmatrix},\ \boldsymbol{D}_2=\begin{bmatrix}\mu^{\mathrm{c}}&0\\ 0&\mu^{\mathrm{c}}\end{bmatrix},$$

A pile foundation mostly comprises a group of piles with a footing on top of them. Therefore, the equilibrium condition between the discrete piles and the continuum soils in this axisymmetric finite element model should be considered carefully. The behavior of piles on the same radius from the center is also approximated by the limited Fourier harmonics of $n=0$ and 1 along the circumferential direction connecting the relevant piles axis. This assumption is reasonable so long as the rings of piles maintain the original axisymmetric configuration during the motion at any depth. In the analysis of the interaction between discrete ring piles and the surrounding continuum soils, the pile element and the neighboring soil element are assumed to have the same translation displacements at the connection nodes. The piles are modeled by the two-node three-dimensional beam elements, and their stiffness is integrated into the soil stiffness.

4.2 Verification of pile foundation–soil interaction model with field tests

Field tests of pile foundations subjected to vertical and horizontal dynamic loadings were conducted in Taiwan high-speed railway to verify the proposed analysis method for pile foundation–soil dynamic interaction. The profile of the pile foundation and its finite element model are shown in Figs. 7 and 8, respectively. The piles are modeled into two rings of beam element, and parameters of the model in Fig. 8 are taken from the literature [21]. Because of the high rigidity of the footing structure, it is regarded as a rigid block in the analysis. The motions of the footing are transferred to the soil nodes and pile nodes at the connecting interface with a master–slave relation. In the numerical computation, the amplitude of the dynamic loading is kept as 10 kN to accord with the output force from the shaker in field tests.

The field test results [21] by the National Earthquake Engineering Center of Taiwan for the pile foundation subjected to shaker loading in Fig. 7 are used to validate the three-dimensional axisymmetric finite element model. In the shaker tests, the output force is proportional to the eccentric

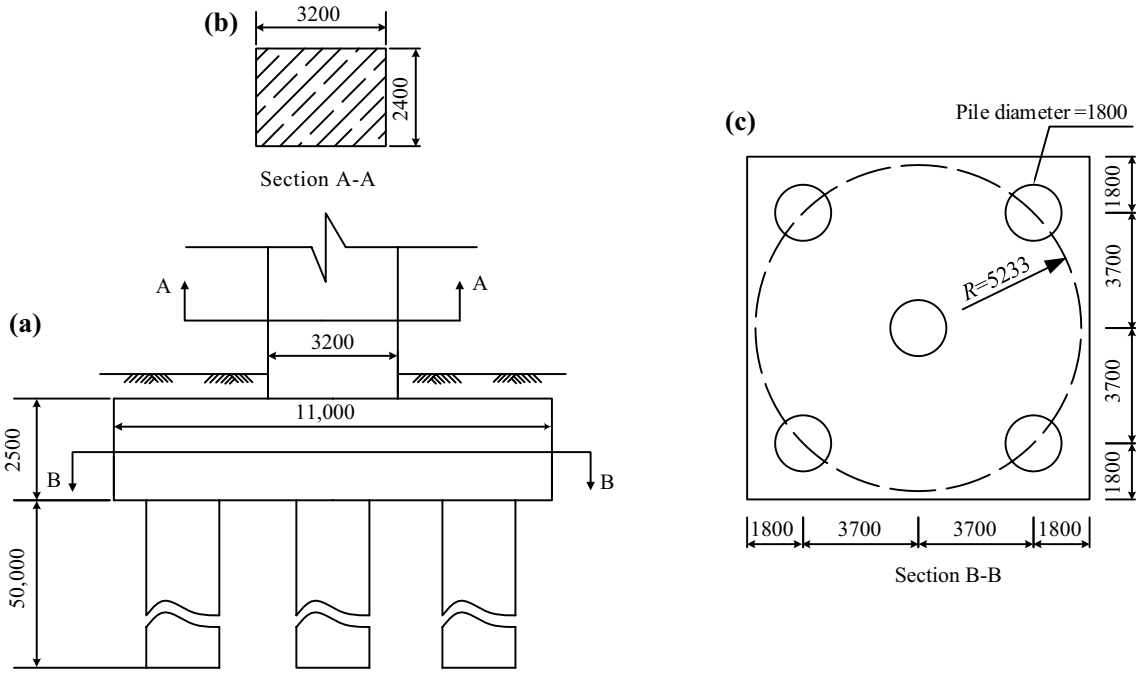

Fig. 7 Pile foundation of Taiwan high-speed railway viaduct (in mm): **a** front view of pile foundation; **b** top view of section A-A; **c** top view of section B-B

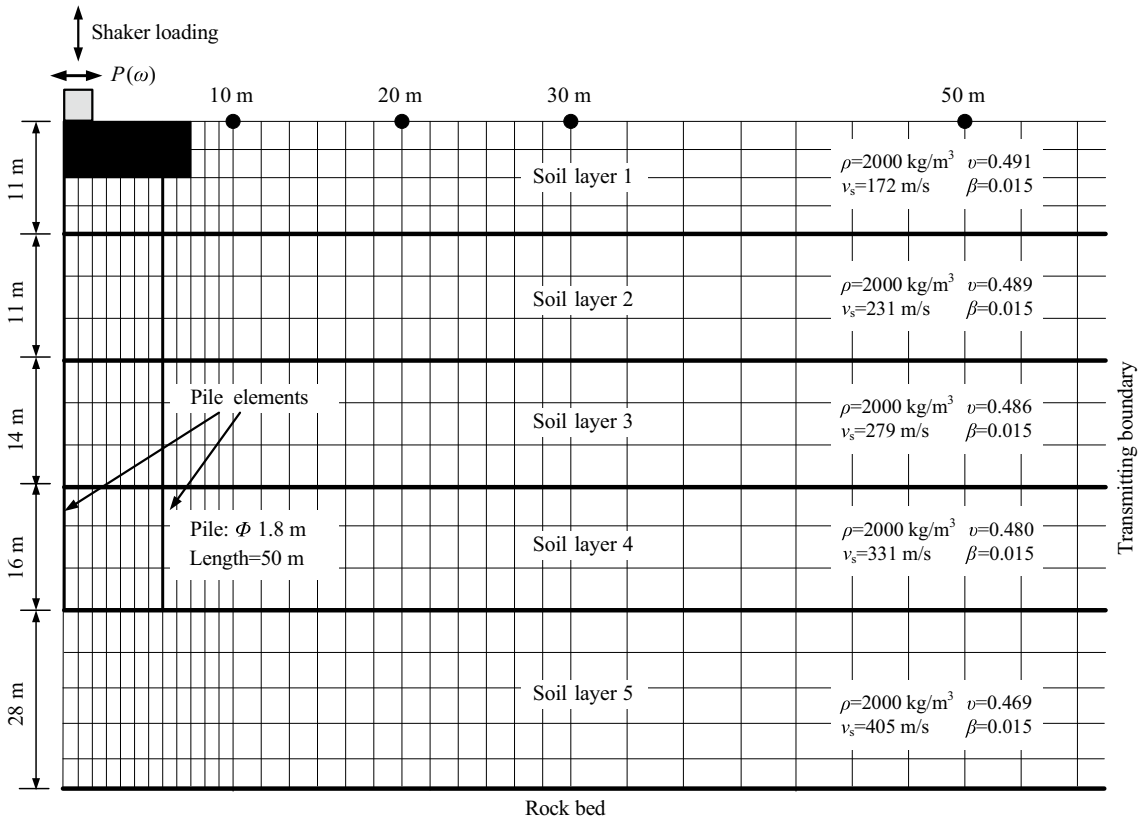

Fig. 8 Axisymmetric finite element model of pile foundation and site condition

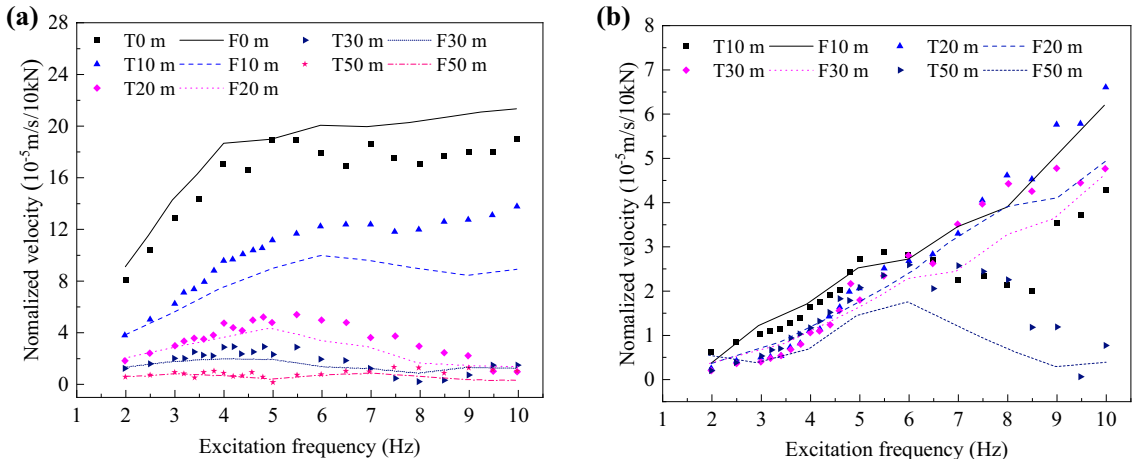

Fig. 9 Comparison of simulated and recorded ground surface velocity responses due to the horizontal loading (prefix 'F' stands for computation results and 'T' for field test data): **a** horizontal velocity responses; **b** vertical velocity responses

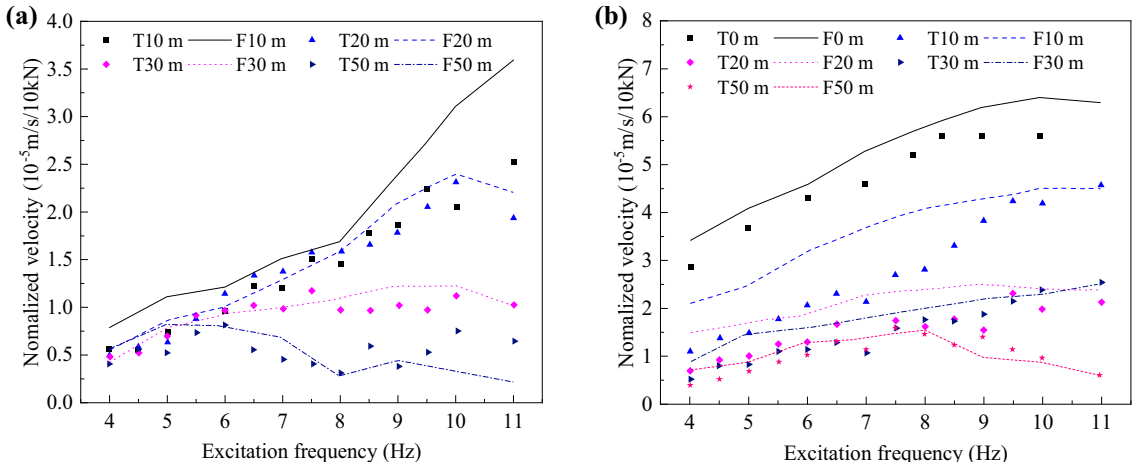

Fig. 10 Comparison of simulated and recorded ground surface velocity responses due to the vertical loading (prefix 'F' stands for computation results and 'T' for field test data): **a** horizontal velocity responses; **b** vertical velocity responses

mass and the square of the test frequency, such that the frequency of input force varies from 2 to 11 Hz, to guarantee that the output force is within the design capacity of the exciter. Either vertical or horizontal loadings was applied at the top of the pile foundation. Since the harmonic exerting force by shakers generally depends on the driving frequency, the measured data were normalized with respect to a fixed maximum excitation force of 10 kN for both the horizontal and vertical directions. The velocity response of ground surface was recorded at the positions of 0, 10, 20, 30, and 50 m from the center of pile foundation. Test results are presented in Figs. 9 and 10 for horizontal and vertical shaker loadings, respectively. The horizontal and vertical velocity of the computed results under horizontal loads and vertical loads is also presented in the same figures for comparison purposes. Generally, the simulation results show reasonable agreement with the field measurements, which proves the reliability of the proposed computation procedure to evaluate ground responses under pile foundation excitations.

5 Validation of the proposed approach by field measurements

5.1 Field tests of Beijing–Tianjin inter-city high-speed railway

The Beijing–Tianjin intercity express railway is one of the newly built high-speed railways in China with an operation speed up to 350 km/h. About 87% of this railway uses viaducts with span lengths of 32 m, which are supported by pile foundation with pile length up to 50 m. Field tests of ground vibrations due to trains running on a viaduct were

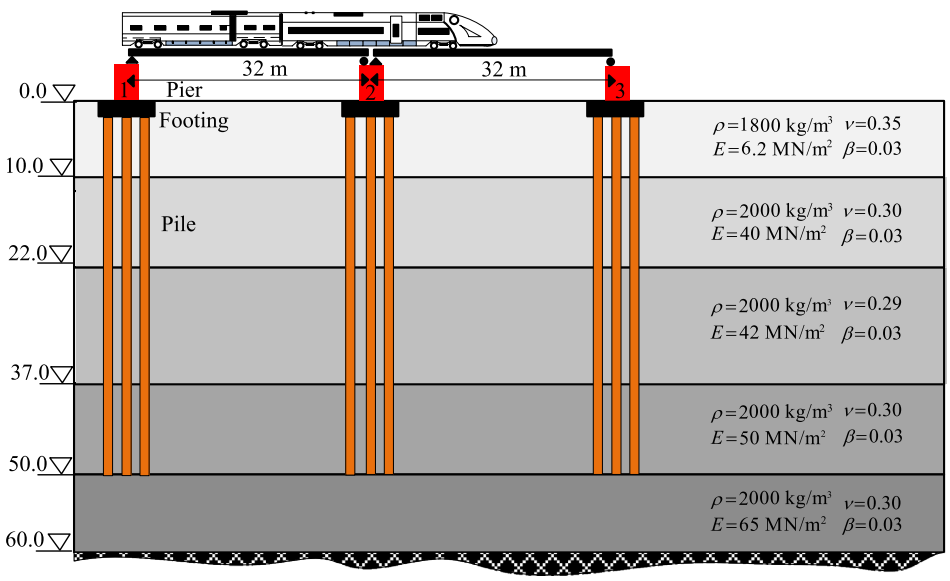

Fig. 11 Test site in Beijing–Tianjin intercity express railway

Table 2 Train parameters

Parameter	Value
Mass of car body m_c	40×10^3 kg
Mass of wheel m_w	1.2×10^3 kg
Moment inertia of car body I_c	5.47×10^5 kg·m^2
Stiffness of primary suspension k_1, k_2	2.08 MN/m
Damping of primary suspension c_1, c_2	200 kN·s/m
Wheelbase l_c	17.5 m

Table 3 Viaduct parameters

Parameter	Value
Beam span L	32 m
Young's modulus of beam E_b	3.5×10^{10} Pa
Moment inertia of beam I_b	11.17 m^4
Mass of beam m_b	22.8×10^3 kg/m

performed. The parameters of pile foundation and site conditions as shown in Fig. 11 are taken from the literature [22, 23]. Observation points at pier top and ground surface in a line perpendicular to the viaduct were selected to record vibrations induced by trains running at different speeds. Distance of these observation points from the pier foot was 10, 20, 30, and 50 m, respectively.

Parameters of train and viaduct structure in the field tests are given in Table 2 and Table 3, respectively. Note that the parameters in Table 1 are in accordance with the case in literature [4], used to validate our proposed model with previous research and here to validate the model by field measurements, so the parameters of train and viaduct are different from the previous case.

Based on the proposed viaduct–pile foundation–soil dynamic analysis model with train moving loads, the computed vibration with time at pier top and on ground surface 20 m from pier foot is plotted in Figs. 12 and 13 for train speeds of 150 and 300 km/h, respectively; field test data at the same locations are plotted in the same figures for comparison. The computed vibrations at these two positions show reasonable agreement with the test data despite some discrepancies. The peak responses due to train wheel axle movement can be easily identified in these results. Both computation results and field test data show that train with a higher speed causes stronger vibrations at the viaduct and nearby ground.

The frequency spectra of the vertical velocities of the pier top and ground surface are shown in Figs. 14 and 15 for train speeds of 150 and 300 km/h, respectively. The computed vibrations at these two positions show reasonable agreement with the test data despite some discrepancy. The difference in the range of 40–80 Hz arises from site conditions. The site conditions in FEM are ideal, while the actual site conditions are complex due to the spatial nonuniformity of soil and the variability of soil damping in each layer. The soil stiffness and damping are variable because the soil shear strain is significantly related to high frequency, which affects the response of ground vibration at high frequency. Both computation results and field test data show that the main frequencies of the pier top are below 100 Hz while the main frequencies of the ground surface are below 30 Hz. It means that the higher-frequency characteristics decay faster than

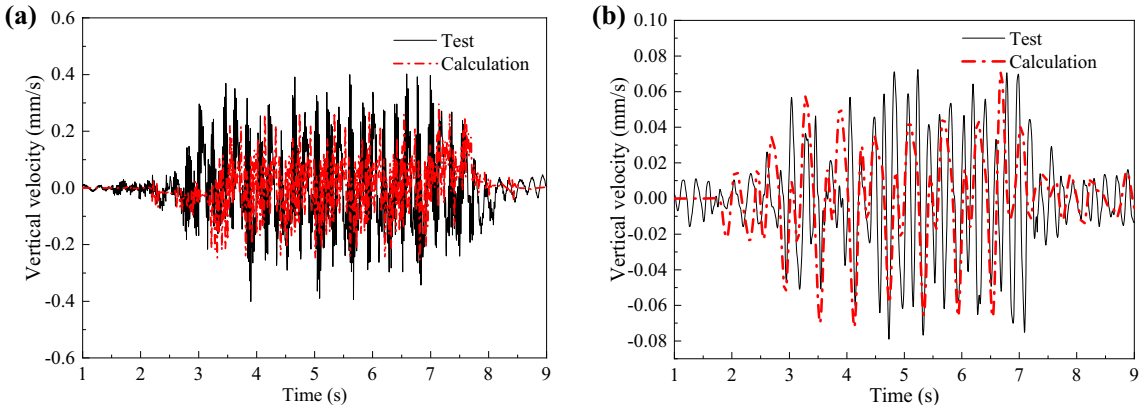

Fig. 12 Vertical responses of the sensors at train speed of 150 km/h: **a** pier top; **b** ground surface 20 m from pier foot

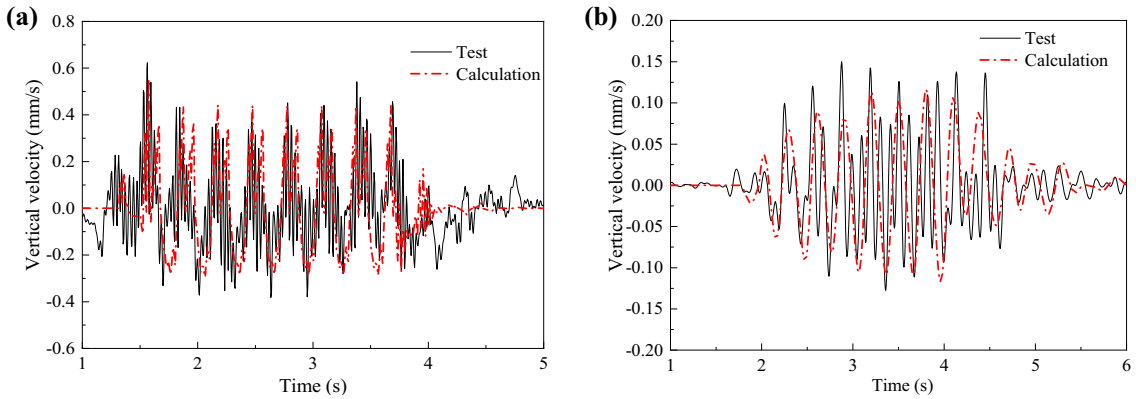

Fig. 13 Vertical responses of the sensors at train speed of 300 km/h: **a** pier top; **b** ground surface 20 m from pier foot

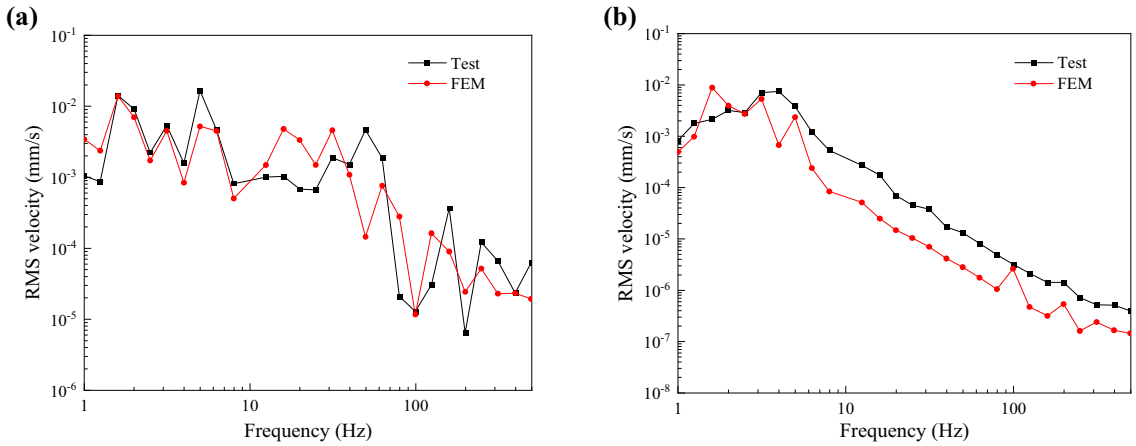

Fig. 14 Frequency spectra of the vibration at train speed of 150 km/h: **a** pier top; **b** ground surface 20 m from pier foot

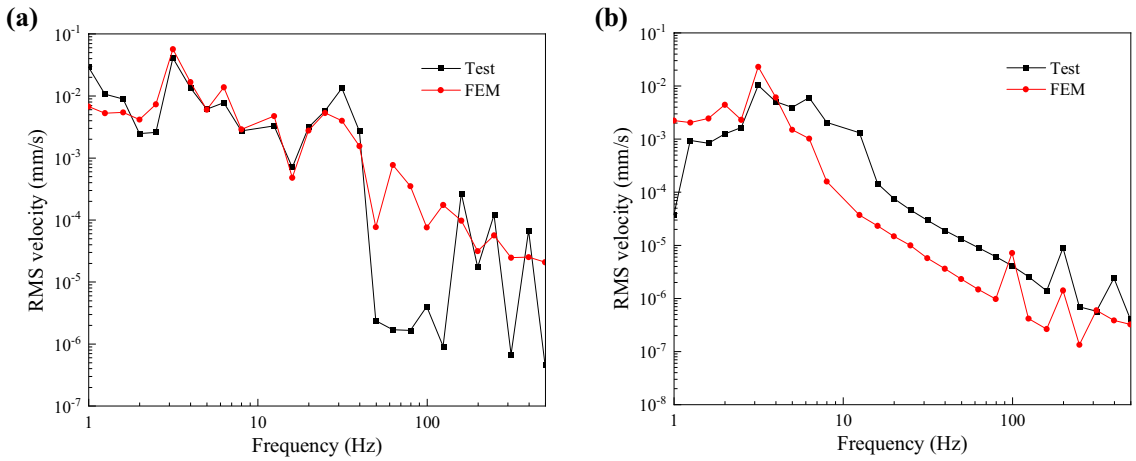

Fig. 15 Frequency spectra of the vibration at train speed of 300 km/h: **a** pier top; **b** ground surface 20 m from pier foot

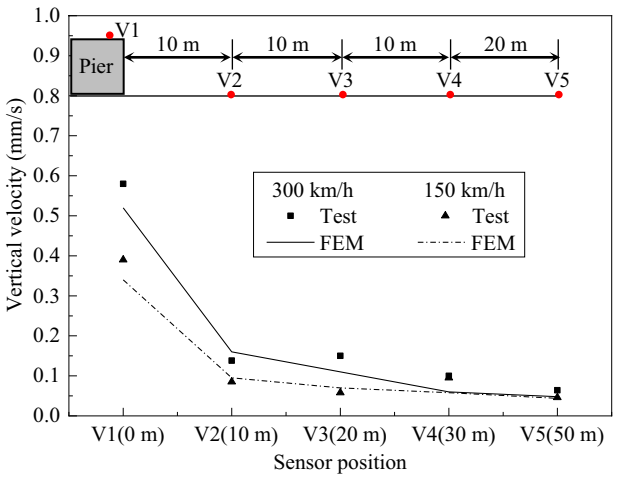

Fig. 16 Attenuation of the vertical vibration at pier top and ground surface with the distance from pier foot

lowers. Figure 16 shows that train speed has noticeable effect on the vibration at pier top and nearby soil, but this effect will diminish with the distance from pier at ground surface.

5.2 Field tests of Shanghai–Hangzhou high-speed railway

The Shanghai–Hangzhou high-speed railway is also one of the newly built high-speed railways in China with an operation speed up to 350 km/h. About 90% of this railway uses viaducts which are supported by pile foundation. Field tests of bridge vibrations due to trains running on a viaduct with a bridge span of 24 m were performed. Observation points at bridge midspan and endspan as shown in Fig. 17 were selected to record the vibrations

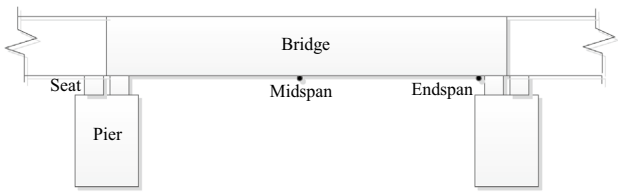

Fig. 17 Test site in Shanghai–Hangzhou high-speed railway

induced by trains running at different speeds. The points at pier top and on ground surface 10 m from the pier foot were also observed.

Based on the proposed viaduct–pile foundation–soil dynamic analysis model with train moving loads, the computed vibration with time at midspan and endspan is plotted in Figs. 18 and 19 for train speeds of 80 and 220 km/h, respectively; field test data at the same locations are also plotted in the same figures for comparison. The computed vibrations at these two positions show reasonable agreement with the test data despite some discrepancy. The peak responses due to train wheel axle movement can be easily identified in these results.

The frequency spectra of vertical velocities at bridge midspan and endspan for train speeds of 80 and 220 km/h are shown in Figs. 20 and 21, respectively. The computed vibrations at these two positions show reasonable agreement with the test data despite some discrepancy.

Vibration reaction at bridge structure due to train running on viaduct is presented in Fig. 22 for two train speeds of 80 and 220 km/h. Both computation results and field test data show a consistent trend of vibration attenuation.

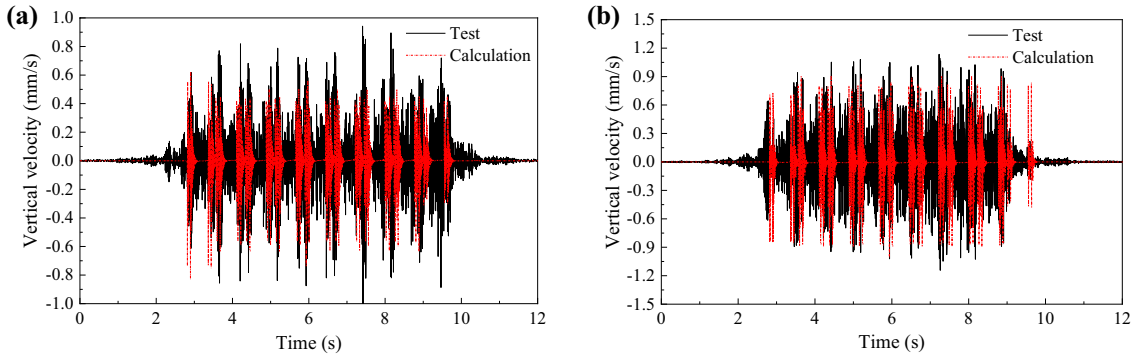

Fig. 18 Vertical response of the sensors at train speed of 80 km/h: **a** midspan; **b** endspan

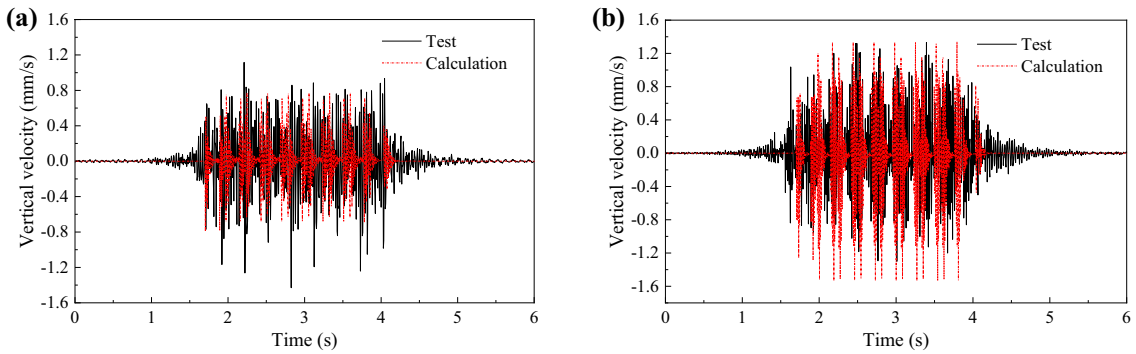

Fig. 19 Vertical response of the sensors at train speed of 220 km/h: **a** midspan; **b** endspan

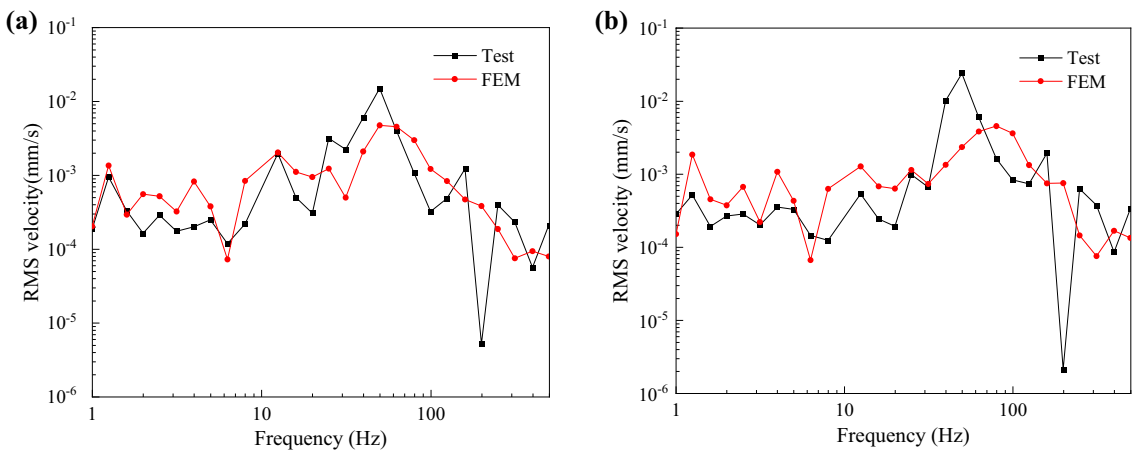

Fig. 20 Frequency spectra of the vibration at train speed of 80 km/h: **a** midspan; **b** endspan

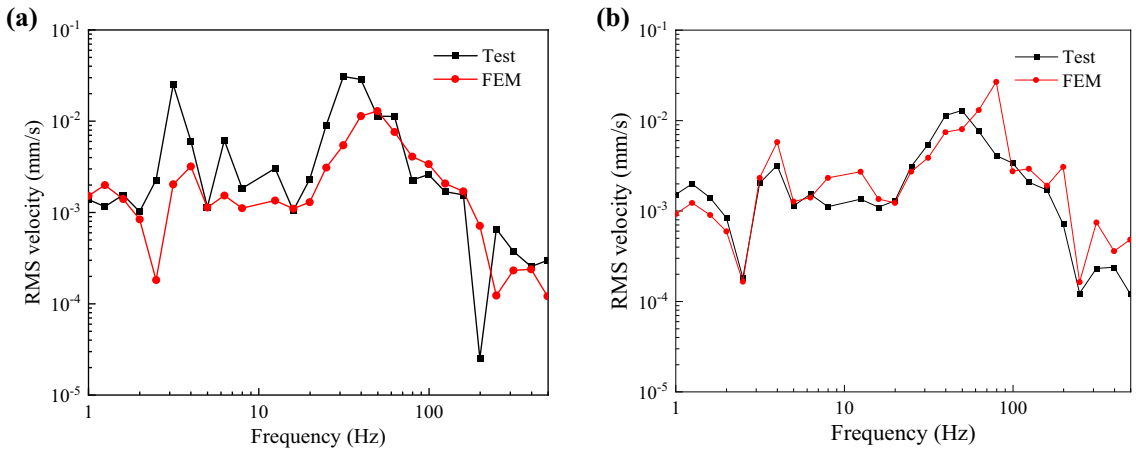

Fig. 21 Frequency spectra of the vibration at train speed of 220 km/h: **a** midspan; **b** endspan

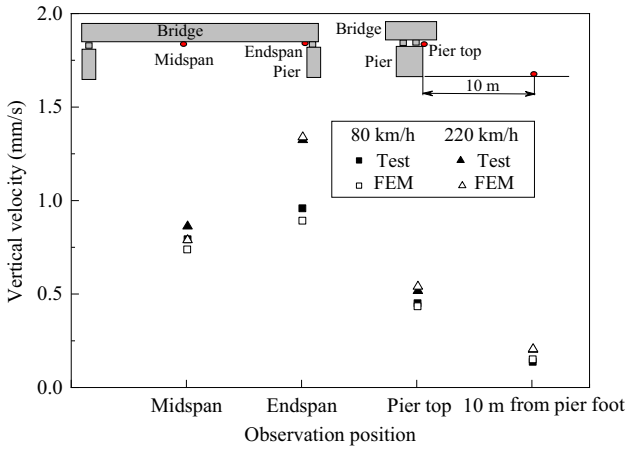

Fig. 22 Attenuation of the vertical vibration at bridge and ground surface

6 Conclusion

An efficient train–viaduct–pile foundation–soil interaction analysis model has been proposed herein to study the ground vibration induced by train running on viaduct. Dynamic substructure method is applied to divide the whole system into two subsystems. The dynamic interaction of the train–viaduct subsystem and the pile foundation–soil subsystem is solved by dynamic stiffness integration method and Fourier series decomposition method, respectively. The three-dimensional problem of pile–soil interaction is decomposed into several two-dimensional axisymmetric finite element models according to the axisymmetric or anti-axisymmetric modes of loads. The two subsystems are coupled with the displacement compatibility condition at interface of viaduct pier bottom and pile foundation via the impedance function at pile foundation top. The proposed analysis model has been applied to evaluate the ground vibrations induced by train moving load on a viaduct in Beijing–Tianjin intercity express railway, and the computed results are compared with field measurements both at pier top and on ground surface. The model has also been applied to evaluate the viaduct vibrations induced by train moving load in Shanghai–Hangzhou high-speed railway, and the computed results are compared with field measurements both at midspan and at endspan. The results of the case studies have demonstrated the applicability and accuracy of the proposed analysis model in viaduct–ground interaction analysis with train moving loads.

Acknowledgements This work was supported by the National Natural Science Foundation of China (Nos. 52125803, 51988101 and 52008369).

References

1. Li Q, Thompson DJ (2018) Prediction of rail and bridge noise arising from concrete railway viaducts by using a multilayer rail fastener model and a wavenumber domain method. Proc Inst Mech Eng, Part F: J Rail Rapid Transit 232(5):1326–1346

2. Li X, Liu Q, Pei S, Song L, Zhang X (2015) Structure-borne noise of railway composite bridge: numerical simulation and experimental validation. J Sound Vib 353:378–394
3. Liu X, Zhang N, Sun Q, Wang Z, Zang C (2022) An efficient frequency domain analysis method for bridge structure-borne noise prediction under train load and its application in noise reduction. Appl Acoust 192:108647
4. Frýba L (1999) Vibration of solid sand structures under moving loads. Thomas Telford
5. Yang YB, Yau JD, Hsu LC (1997) Vibration of simple beams due to trains moving at high-speeds. Eng Struct 19(11):936–944
6. Zeng ZP, Liu FS, Wang WD (2022) Three-dimensional train–track–bridge coupled dynamics model based on the explicit finite element method. Soil Dyn Earthq Eng 153:107066
7. Gou H, Zhao T, Qin S, Zheng X, Pipinato A, Bao Y (2022) In-situ testing and model updating of a long-span cable-stayed railway bridge with hybrid girders subjected to a running train. Eng Struct 253:113823
8. Cheng YS, Au FTK, Cheng YK (2001) Vibration of railway bridges under a moving train by using bridge–track–vehicle element. Eng Struct 23(12):1597–1606
9. Cheng YS, Au FTK, Cheung YK, Zheng DY (1999) On the separation between moving vehicles and bridge. J Sound Vib 222(5):781–801
10. Cheung YK, Au FTK, Zheng DY, Cheng YS (1999) Vibration of multi-span bridges under moving vehicles and trains by using modified beam vibration functions. J Sound Vib 228(3):611–628
11. Zhai W, Wei K, Song X, Shao M (2015) Experimental investigation into ground vibrations induced by very high-speed trains on a non-ballasted track. Soil Dyn Earthq Eng 72:24–36
12. Ren X, Wu J, Tang Y, Yang J (2019) Propagation and attenuation characteristics of the vibration in soft soil foundations induced by high-speed trains. Soil Dyn Earthq Eng 117:374–383
13. Feng SJ, Zhang XL, Wang L, Zheng QT, Du FL, Wang ZL (2017) In situ experimental study on high speed train induced ground vibrations with the ballast-less track. Soil Dyn Earthq Eng 102:195–214
14. Li J, Chen S, Yu F, Dai Z, Ojekunle OV (2020) In situ model tests to investigate the dynamic response of water-softened subgrade under vibrating loads. Soil Dyn Earthq Eng 138:106336
15. Zhang Y, Li L, Lei Z, Yu L, Bu Z (2021) Environmental noise beside an elevated box girder bridge for urban rail transit. J Zhejiang Univ-Sci A 22(1):53–69
16. Shi L, Sun H, Pan X, Geng X, Cai Y (2019) A theoretical investigation on characteristic frequencies of ground vibrations induced by elevated high speed train. Eng Geol 252:14–26
17. Takemiya H, Bian XC (2007) Shinkansen high-speed train induced ground vibrations in view of viaduct–ground interaction. Soil Dyn Earthq Eng 27(6):506–520
18. Fujikake TA (1986) Prediction method for the propagation of ground vibration from railway trains. J Sound Vib 111(2):357–360
19. Takemiya H, Yamada Y (1981) Layered soil–Pile–Structure dynamic interaction. Earthquake Eng Struct Dynam 9(5):437–457
20. Takemiya H (1986) Ring pile analysis for grouped piles subjected base motion. Struct Eng Earthquake Eng 3(1):195–202
21. Lin TW, Chen CH and Lee YJ (2000) Vibration studies for Tainan Science Park due to high-speed train. Evaluation of vibration reduction of train viaduct. National Earthquake Engineering Center Report, NCREE-00–001 (**in Chinese**)
22. Gao GY, Chen GQ, Li J (2014) Numerical analysis of dynamic characteristic of transversely isotropic saturated soil foundation subjected to high-speed train load. Chin J Rock Mech Eng 33(1):189–198 (**in Chinese**)
23. Sun SL, Zhang WJ, Wang ZH, Su W, Wu CL, Bu QH (2009) Design of unballasted track bridges in Beijing–Tianjin intercity railway. Strategic Study of CAE 11(1):32–42 (**in Chinese**)